Exploring the formation and evolution of planetary systems
Proceedings IAU Symposium No. 299, 2013
A.C. Editor, B.D. Editor & C.E. Editor, eds.
© 2013 International Astronomical Union
DOI: 00.0000/X000000000000000X

First high-angular resolution L' images of the β Pictoris debris disc with the VLT / NaCo

Julien Milli[1,2], Dimitri Mawet[1], Olivier Absil[3], Anne-Marie Lagrange[2], Jean-Charles Augereau[2] and Julien H. Girard[1]

[1]European Southern Observatory, Casilla 19001, Santiago 19, Chile, email: jmilli@eso.org

[2]Institut de Planetologie et d'Astrophysique de Grenoble, CNRS, BP 53, 38041 Grenoble, France

[3]Departement d'Astrophysique, Geophysique et Oceanographie, Universite de Liege, 17 Allee du Six Aout, B-4000 Liege, Belgium

Abstract. Imaging debris discs in the L'-band (3.8 μm) is difficult a task. Quasi-static speckles from imperfect optics prevail below 1″whereas background emission is the dominant noise source beyond that separation and is much larger than at shorter wavelengths . We demonstrate here the potential of the newly commissioned AGPM coronograph on VLT/NaCo combined with advanced star and sky subtraction technique based on Principal Component Analysis, and we analyze the morphology of the β Pictoris disc.

Keywords. β Pictoris, high-angular resolution, Annular Groove Phase Mask coronograph, Principal Component Analysis

1. Introduction

Circumstellar discs are the birthplace of planets, especially the disc inner regions within a few tens of astronomical units. Therefore imaging discs at that scale helps to constrain the planet formation mechanisms. This requires high-contrast and high-angular resolution techniques as well as specific data reduction tools. Innovative methods such as Angular Differential Imaging, ADI (Marois et al. 2006), Locally-Optimized Combination of Images, LOCI (Lafrenière et al. 2007) and Principal Components Analysis, PCA, Soummer et al. (2012) or Amara & Quanz (2012) were developed to detect and characterize faint companions. They are well suited for imaging point sources. For discs, they are also used to reveal high spatial frequency features (Buenzli et al. (2010), Thalmann et al. (2011) or Lagrange et al. (2012)) but any extended structure is strongly biased (Milli et al. 2012). On the specific example of the β Pictoris system imaged with the VLT/NaCo, we present here a way to correct the biases induced by ADI and analyze the morphology of the disc in the L'-band.

2. Observations and data reduction specific to the disc geometry

The star β Pictoris was observed on January, 31 2013 during the science verification observing run of NACO's new AGPM coronagraphic mode (Absil et al. 2013 in preparation). The AGPM coronograph operates in the L'-band at 3.8 μm with an undersized Lyot stop blocking the light from the secondary mirror and telescope spiders (Mawet et al. 2013). The main source of noise that needs to be overcome to reveal faint extended emission beyond 1″ comes from the high background sky and telescope emission at this wavelength. The background as evaluated by manual offsets on an empty region of the sky with the adaptive optics loop (AO) opened did not give satisfactory results in terms of background subtraction. The main reason comes from the fact that the thermal emission of the deformable mirror varies whether the AO loop is opened or closed. Therefore the cosmetic treatment of the raw data only consisted in dark subtraction, flat-field correction and bad-pixel interpolation without any background subtraction. The data were

binned every 100 second, resulting in a data cube of 90 images. The star subtraction algorithm consisted in a PCA performed in four concentric annuli between 0″, 0.27″, 0.5″, 1″ and 5.1″, retaining 5 components out of 90. The reduced image is shown in Fig. 1. The disc is detected from 0.5″ to 4.5″ at a mean 3σ level. Low frequency noise due to strong background emission prevent any detection further away. On the South-West side, the strong background emission beyond 3″ bows the disc towards the East and makes the disc artificially brighter at that separation. The warp seen at smaller wavelength between 3 and 5″ (Lagrange et al. 2012) is only seen on the South-West side. To be able to decide between artificial and physical features, we also reduced NaCo archival non-coronographic data of the disc in the same band, taken in September, 28 2010. The same reduction and analysis was performed on this dataset. Although the low-frequency background noise is lower , the observing strategy implied telescope offsets that limits the field of view. Therefore the disc is detected only up to 3.5″. Moreover, below 1″, bright speckles and diffraction residuals from the telescope spiders prevent any clear conclusion.

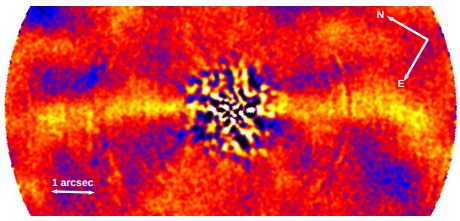

Figure 1. Coronographic image. The planet is seen on the North-West side.

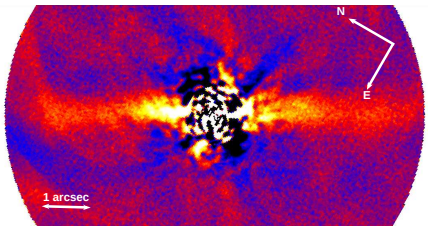

Figure 2. Non-coronographic image. Residuals are greater at short separation

3. Morphological analysis

As a first step, the image was derotated to align each side horizontally. We estimated the position angle (PA) of the disc midplane by a least-squares fitting under the assumption that the disc has its maximum intensity along the midplane, as already performed e.g. in Lagrange et al. (2012). We used a Lorenzian profile as the fitting function, and nulled the mean spine center between 1″ and 3″. The measured PA is 28.3° ± 2° and 212.3° ± 2° on the coronographic image (respectively 29.0° ± 2° and 211.3° ± 2° on the non-coronographic image). The surface brightness distribution (SBD) corrected from the flux losses related to ADI (see section 4) is displayed in Fig. 3. The two dat sets agree on a smooth slope of the SBD. The brightness asymmetry detected in the coronographic image is not confirmed on the non-coronographic image.

4. Modelisation of the disc and correction of the ADI biases

ADI may heavily bias signal extraction of extended objects (Milli et al. 2012) (Milli et al. 2012). Therefore a careful calibration of flux losses was performed using discs model generated with the GRaTeR code (Augereau et al. 1999). In order to limit the parameter space, we assumed a radially symmetric distribution of optically thin dust with constant scattering cross-section. The dust vertical distribution is assumed to be gaussian with a 2AU scale height at the radius r_0 and a flaring exponent $\beta = 1.5$. The radial profile is described by two power laws of exponents $\alpha_{in} = 2$ and α_{out} with a peak density at the radius r_0. The disc model is subtracted from the initial data cube, and the resulting cube is re-reduced using PCA. This step is repeated iteratively by varying the free parameters of the disc model, namely the PA, α_{out}, r_0, and the peak density, until the residuals are minimized in the disc region. The minimization algorithm used is an amoeba. We performed this minimization for three different disc inclinations with respect to the line of sight

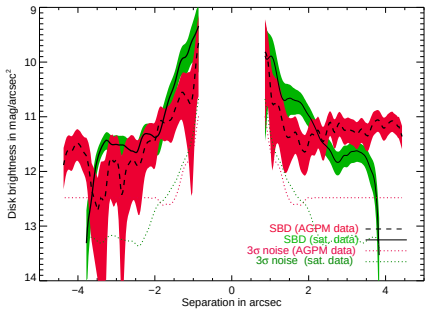

Figure 3. Disc brightness as obtained from fitting a Lorentzian profile along the disc vertical profiles. The coloured region show the measurement error. The North-East is on the right.

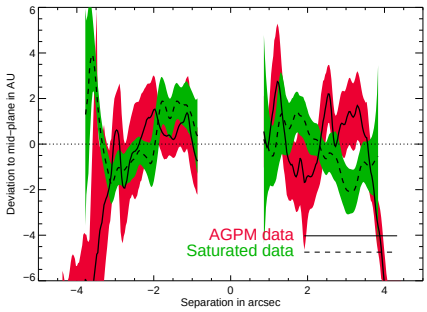

Figure 4. Position of the disc midplane, e.g. vertical offset of the Lorentzian profile relative to the mean disc position angle. The North-East is on the right.

Table 1. Average of the best model parameters for the AGPM and saturated data.

Scattering model	inclination	PA	r_0	α_{out}
isotropic	91°	30.3° ± 1°	30.5 ± 20	−0.3 ± 0.2
isotropic	95°	30.3° ± 0.8°	35.6 ± 20	−0.7 ± 0.2
isotropic	100°	31.2° ± 1.8°	34.6 ± 9	−1.1 ± 0.2
anisotropic	91°	30.3° ± 1.1°	30.5 ± 22	−0.3 ± 0.3
anisotropic	95°	29.8° ± 2.0°	30.5 ± 10	−0.3 ± 0.3

(91°, 95° and 100°) and two models: an isotropic-scattering model and an anisotropic-scattering model with a Henvey Greenstein parameter $g = 0.5$. The best model parameters are presented in Table 1, they represent an average of the best models obtained for the coronographic and the non-coronographic image for two different PCA settings. The uncertainty represents the dispersion in those results. The best reduced χ^2 were obtained with an isotropic model of a disc inclined at 95° and 100°. Larger inclinations fit better the observation for an isotropic model, unlike anisotropic models. It should be noted that the peak density radius r_0 is poorly constrained by the observation hence a large uncertainty. The disc PA obtained by this modeling approach agrees within error bars with the direct measurement presented in Section 3. The best disc models were used to compute the flux losses resulting from PCA reduction and to correct the SBD displayed in Fig. 3 from the ADI biases.

References

Amara, A. & Quanz, S. P. 2012, MNRAS, 427, 948
Augereau, J. C., Lagrange, A. M., Mouillet, D., Papaloizou, J. C. B., & Grorod, P. A. 1999, A&A, 348, 557
Buenzli, E., Thalmann, C., Vigan, A., et al. 2010, A&A, 524, L1
Lafrenière, D., Marois, C., Doyon, R., Nadeau, D., & Artigau, É. 2007, ApJ, 660, 770
Lagrange, A.-M., Boccaletti, A., Milli, J., et al. 2012, A&A, 542, A40
Marois, C., Lafrenière, D., Doyon, R., Macintosh, B., & Nadeau, D. 2006, ApJ, 641, 556
Mawet, D., Absil, O., Delacroix, C., et al. 2013, A&A, 552, L13
Milli, J., Mouillet, D., Lagrange, A.-M., et al. 2012, A&A, 545, A111
Soummer, R., Pueyo, L., & Larkin, J. 2012, ApJ, 755, L28
Thalmann, C., Janson, M., Buenzli, E., et al. 2011, ApJ, 743, L6